

Article

Influence of a Scanning Radial Magnetic Field on Macroparticle Reduction of Arc Ion-Plated Films

Shuhao Wang, Zeng Lin *, Hong Qiao, Dechun Ba and Lida Zhu

School of Mechanical Engineering & Automation, Northeastern University, Shenyang 110004, China; m15940597879@163.com (S.W.); 159753qh@163.com (H.Q.); dchba@mail.neu.edu.cn (D.B.); neulidazhu@163.com (L.Z.)

* Correspondence: zlin@mail.neu.edu.cn; Tel.: +86-24-8367-6945

Received: 24 November 2017; Accepted: 23 January 2018; Published: 25 January 2018

Abstract: Cathode spot motion influences the physical characteristics of arc plasma and the related macroparticles (MPs) in resultant films; these MPs limit the application of arc ion plating (AIP). In this paper, a scanning radial magnetic field (SRMF) was applied to the cathode surface to control the cathode spot motion and reduce the MP contamination in the deposited films. It was shown that film surface morphologies prepared using SRMF were better than those using a static radial magnetic field (RMF). The improvement was greater with increased scanning range and frequency. Using SRMF, cathode spot motion was confined to a spiral trajectory on the cathode surface and the spots moved over a large area and at a fast-moving velocity. Both the large moving area and the fast velocity decreased the temperature on the cathode surface and thus reduced the emission of the MPs.

Keywords: scanning radial magnetic field; macroparticle reduction; arc ion plating; cathode spot motion; temperature distribution

1. Introduction

Arc ion plating (AIP) has been widely utilized to deposit various kinds of hard and functional films [1–3]. The cathodic arc used in AIP is a low-voltage, high-current plasma discharge that is produced from an active cathode arc spot with high current density (about 10^5 – 10^7 A/cm²) [2]. The high current density in the cathode spot brings AIP some advantages, such as high ionization rate, high particle energy and good film-matrix adhesion [4,5]. However, it also causes some problems, in particular macroparticle (MP) contamination in deposited films. MPs increase the roughness and porosity of AIP films, which seriously affect film performance [6] and are the biggest obstacle for the practical application of AIP.

Two major methods are used to eliminate MP contamination. The first is to magnetically filter the MPs from the plasma during transport [7,8]. While this method can effectively eliminate MP contamination, it greatly decreases deposition rate and dramatically increases coating costs [9–11]. The second method is using different magnetic field configurations to control cathode spot motion on the cathode surface. Swift [12] proposed that the number and total mass of MPs emitted from a cathode spot was proportional to the cathode spot volume and the cathode spot radius was inversely proportional to the cathode spot speed which was determined by the transverse component of the steering magnetic field. So using the magnetic field reduces contamination by suppressing MP emission from the cathode. This method has more potential for application [13,14]. Among the different magnetic field configurations, the radial magnetic field (RMF) [15] is one of the simplest and most widely used structures, in which the cathode spot velocity can be increased to reduce MP emission. However, using RMF, the cathode spot is confined to a certain orbit, which results in extremely low utilization rate of the cathode material. To avoid this drawback, a dynamic magnetic field (DMF) has been proposed to expand the area on which the cathode spot moves on the cathode surface [14]. There are

several ways to obtain a DMF. One such method involving mechanically moving permanent magnets located adjacent the cathode was proposed by Ramalingam [16]. This type of DMF is modified with a solenoid-generated magnetic field to selectively reinforce or reduce the magnetic field strength normal to the cathode surface. Another method is using a constantly changing electromagnetic field. This type of DMF is modified by adjusting the excitation of the electromagnetic coil [13,14]. Although such kinds of DMFs have been proposed, there is not enough research about the influence mechanism of the DMF on MP reduction. Lang [14] proposed that dynamically controlled cathode spot motion would improve arc discharge and reduce particle emission. However, he did not study the mechanism systematically. In this paper, a DMF configuration using a scanning radial magnetic field (SRMF) was used as the external magnetic field near the cathode.

To explain the influence of SRMF on MP reduction and cathode spot motion, some other factors should be known. Zhirkov et al. [17] reported that a correlated transformation of the arc from Type 2 to the Type 1 was found to be a function of Nitrogen pressure and at.% of Al in the cathode and a reduction in MP generation was found when decreasing Al content and increasing Nitrogen pressure. Jüttner [18] reported the crater size increased at high cathode temperature and large craters explained the enhanced production of large droplets. Anders [19] proposed that the cathode spot velocity increased with the arc current. Utsumi and English [20] found an independence of the MP distribution on the arc current, when studying a range of very small arc current, 2–6 A. Going to a much higher current range, 2–5 kA, Gellert and Schade [21] found a strong dependence of the MP distribution on the current level, which they associated with anode activities. Considering these factors, some measures were taken to avoid the possible influences on the experiment results. In this work, a pure titanium disc was used as the cathode and the Nitrogen pressure kept a low value. There was no heating device for the cathode and the cathode was cooled evenly by water. The arc current remained constant for each group of experiment. Then the trajectory of the cathode spot in the magnetic field was recorded and the velocity was calculated. The temperature distribution on the cathode surface and the MP contamination were characterized. Finally, the influence of SRMF on MP reduction was explained by establishing a correlation between the cathode spot motion features within magnetic field and the MP generation mechanism.

2. Experimental Procedure

A schematic diagram of the experimental apparatus is shown in Figure 1. The apparatus included a vacuum chamber, an arc source and an observation window. In the arc source, a titanium disc (99.99% purity) of 160 mm in diameter, 18 mm in thickness was used as the cathode. A cathode carrier, made of copper was placed behind the cathode. The carrier had an internal chamber accommodating water for cooling. The cooling water was flowing and its temperature was kept constant. The material of the observation window was SiO₂ (99.99% purity). A blocking component was placed in front of the observation window for preventing the MPs and cathode ions coating on the window. This component can be turn on/off outside the vacuum chamber. The magnetic field configuration of the arc source and the distribution of magnetic field lines were shown in Figure 2. The magnetic field was produced at the cathode surface by superimposing the field produced from a coil with adjustable current placed in front of the cathode and 116 cylindrical permanent magnets at the back of the cathode. The coil was made of 2000 loops of 1 mm diameter copper wire. Each permanent magnet was 10 mm in diameter, 12 mm in height and the residual magnetization intensity was 1.4 T. Other parameters of the coil and permanent magnets such as distance from the cathode were shown in Figure 2. It is also seen in Figure 2 that the direction of the axial component of coil field was set to oppose that of permanent magnets. The SRMF in this configuration was produced by periodically changing the coil current. Scanning range, scanning waveform and scanning frequency were three main parameters to control the SRMF distribution.

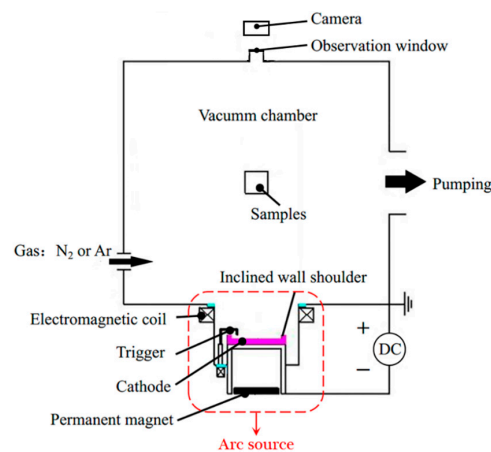


Figure 1. Schematic diagram of the experimental apparatus of the AIP.

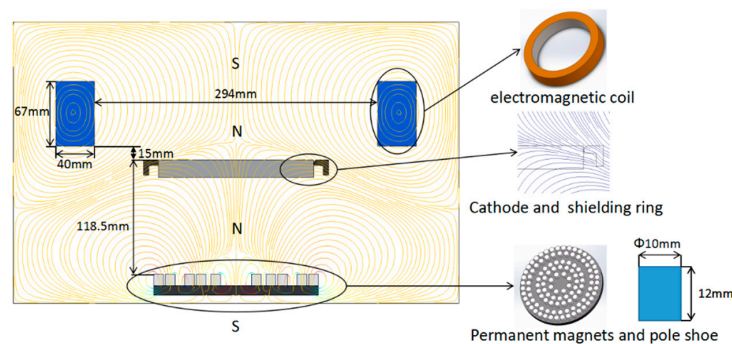
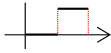


Figure 2. Schematic diagram of the magnetic field configuration of the arc source and the distribution of magnetic field lines.

TiN films were deposited on square stainless-steel substrates with 15 mm length and 2 mm thickness to characterize the film surface properties. Six groups were used and the details of magnetic field parameters for each group are listed in Table 1. The single substrate for each group was located on the axis with a distance of 65 cm away from the cathode. The other coating parameters were as follows: 0.6 Pa Nitrogen pressure, -200 V substrate bias voltage, 100 A cathode current and 60 min deposition time. Prior to the deposition process, the specimen was further cleaned through Argon glow discharges for 10 min, using a bias voltage of -500 V. During deposition, the cathode spot motion and the cathode temperature were monitored through the observation window.

A single lens reflex (SLR) camera (Sony ILCE-5000, Sony Corporation, Tokyo, Japan) was used to record the cathode spot trajectory, and the cathode spot velocity was calculated by the images recorded through a high-speed camera (MEMRECAM (GX-3), NAC, Tokyo, Japan) with an exposure time of $100 \mu\text{s}$. The temperature distribution on the cathode surface was photographed by a thermal camera (Camlink OK AM1460, Beijing JoinHope Image Technology Ltd., Beijing, China) with an exposure time of 50 ms. The transmission in the relevant wavelengths for the thermal camera was 780 nm. The temperature images were obtained with an arcing time 60 min and the arc was still operating. The time interval between two experiment groups was two hours to sufficiently cool the cathode. All the cameras were placed with a distance of 30 cm away from the observation window. The magnetic field distribution on cathode surface under different parameters was measured with a Gauss meter (SJ3000, SenJie Technology, Shenzhen, China). The surface morphology was observed by using a scanning electron microscope (SEM, INSPECT F50, Thermo Fisher Scientific, Eindhoven, The Netherlands). The density and diameter distribution of MPs were quantitatively analyzed with image analysis software (ImageJ 1.47).

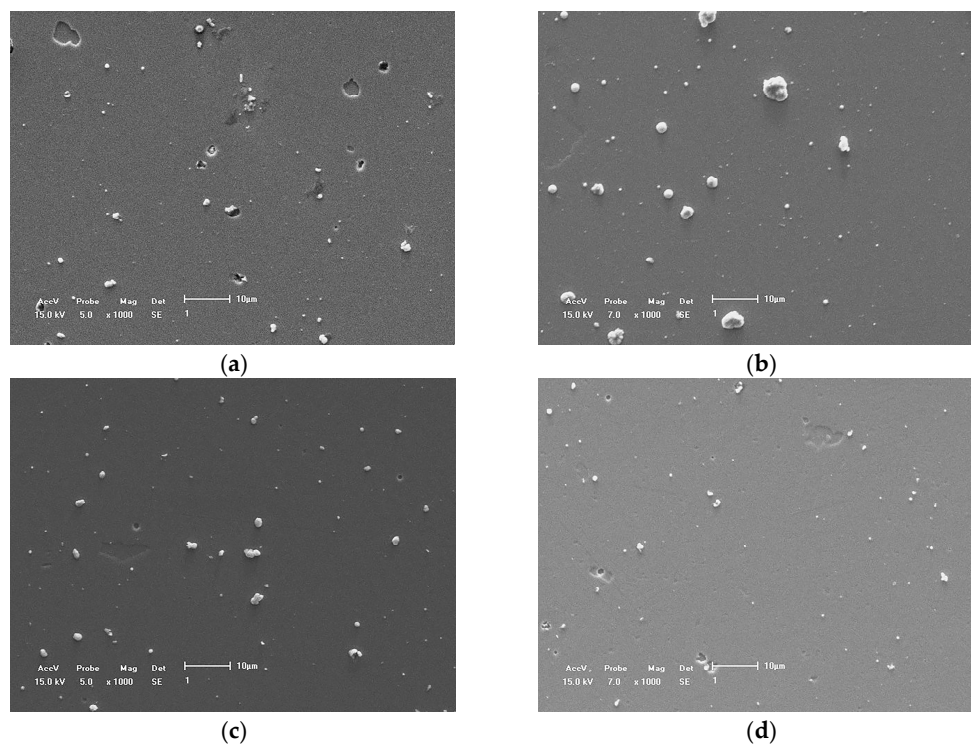
Table 1. Coating experiment magnetic field parameters.

Group	Coil Current (A)	Scanning Frequency (Hz)	Scanning Waveform
1	0.23	–	–
2	0.69	–	–
3	0–0.69	1	
4	0–0.69	5	
5	0–0.92	5	
6	0–0.92	10	

3. Results

3.1. MP Contamination

Typical SEM micrographs of TiN films deposited with different magnetic field parameters are shown in Figure 3. It can be seen from Figure 3 that there was an obvious variation of density and diameter of MPs with magnetic field parameters. Figure 4 shows a statistics of overall quantity and average particle diameter of the SEM micrographs from Figure 3. The minimum diameter of the counted MPs was 1 μm . It can be seen from Figure 4 that: (1) the overall quantity of MPs with coil current 0.23 A were similar to that with current 0.69 A, but there was an obvious decrease on average diameter of MPs in comparison with that of current 0.69 A; (2) the overall quantity and average diameter of MPs decreased with the scanning frequency, when the scanning range was fixed; (3) the overall quantity and average diameter of MPs greatly decreased with the scanning range; (4) overall quantity and average diameter of MPs in the SRMF mode were less than those in the RMF mode.

**Figure 3.** Cont.

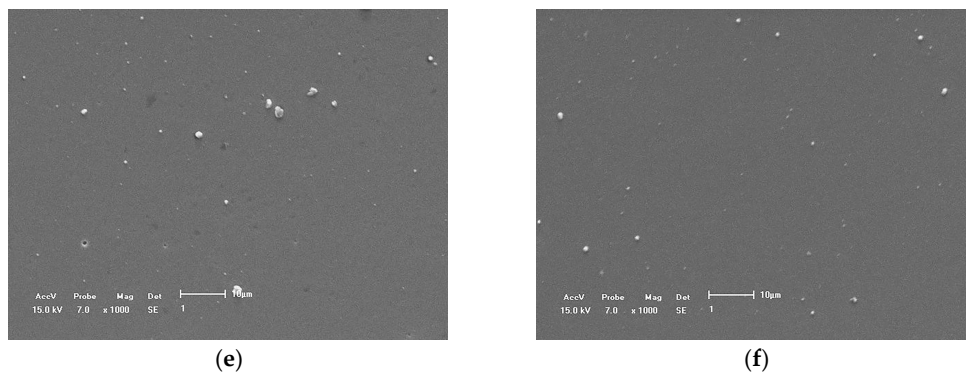


Figure 3. SEM micrographs of the MPs on the TiN film surfaces with different magnetic fields: (a) coil current 0.23 A; (b) coil current 0.69 A; (c) scanning range 0–0.69 A, scanning frequency 1 Hz; (d) scanning range 0–0.69 A, scanning frequency 5 Hz; (e) scanning range 0–0.92 A, scanning frequency 5 Hz; (f) scanning range 0–0.92 A, scanning frequency 10 Hz.

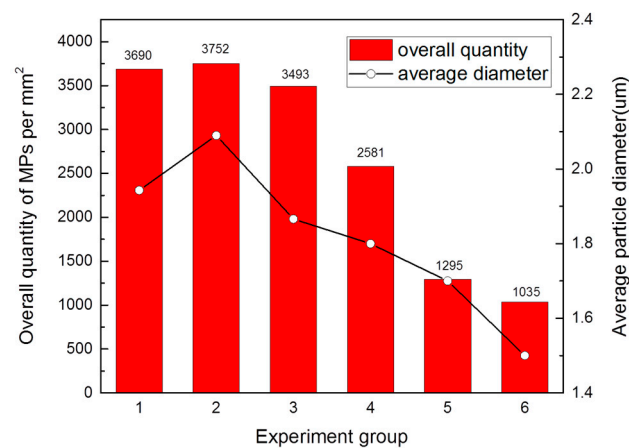


Figure 4. Overall quantity and average diameter of the MPs on the TiN film surfaces with different magnetic fields.

3.2. Magnetic Field Intensity Distribution

Magnetic field intensity distributions produced by different coil currents were measured by a Gauss meter. Figure 5a shows the positions sampled of the cathode surface and the positive direction of axis magnetic field intensity B_N and radial magnetic field intensity B_T . Figure 5b,c show the distributions of axial and radial magnetic field intensity produced by different coil currents. It can be seen in Figure 5b that the intensity of axial component B_N decreased from the center to the edge of cathode surface, when the current was 0 A. When the current increased from 0 to 0.92 A, the intensity of B_N decreased in the negative direction first and then increased in the positive direction. Figure 5c shows that the intensity of B_T increased from the center to the edge of cathode surface and also increased with the coil current. Figure 5d presents the variation of radial magnetic field intensity at the cathode spot trajectory with different coil currents. It can be found that the intensity first increased then decreased with the coil current and the peak appeared at 0.23 A.

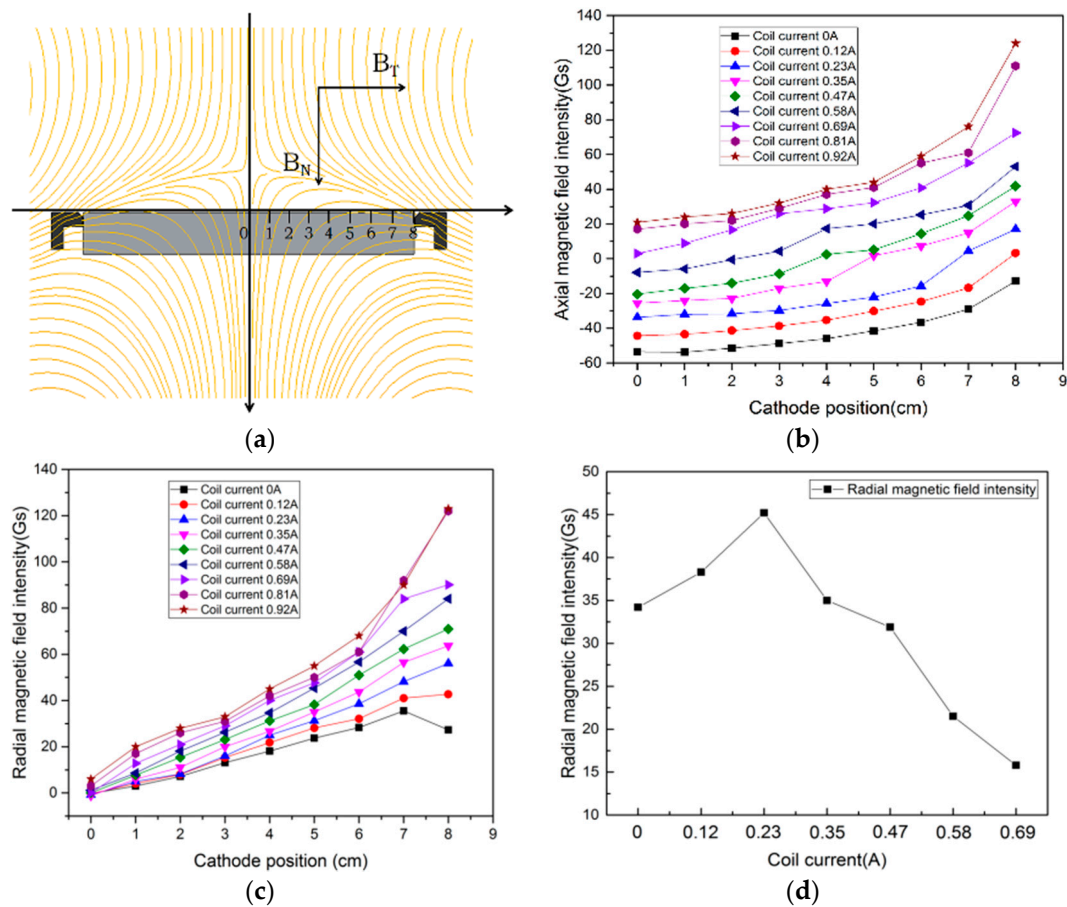


Figure 5. Magnetic field intensity: (a) positions sampled on the cathode surface and the positive direction of axial magnetic field B_N and radial magnetic field B_T ; (b) the distribution of axial magnetic field intensity under different coil currents; (c) the distribution of radial magnetic field intensity under different coil currents; (d) the radial magnetic field intensity at the cathode spot trajectory under different coil currents.

3.3. Cathode Spot Motion

Two aspects of the cathode spot motion were studied: the cathode spot trajectory and the cathode spot velocity. The cathode spot trajectory was recorded by a SLR camera. Figure 6a shows a schematic diagram of the area over which the cathode spot moved on the cathode surface. This area was divided into three parts: edge, middle and central. If the coil current intensity was less than 0.23 A, the cathode spot moved in the edge area of cathode surface, as shown in Figure 6b. In addition, if the coil current intensity was higher than 0.69 A, the cathode spot moved in the central area of cathode surface, as shown in Figure 6c. Figure 7 shows the cathode spot trajectory radius as a function of coil current. It can be seen the trajectory radius decreased gradually when the coil current was increased from 0.23 to 0.69 A. In the SRMF mode, the cathode spot motion was divided into four stages and the trajectory showed three forms as shown in Figure 6d–f. Trajectory form 1 was a circle in the edge area of cathode surface; trajectory form 2 was a spiral in the middle area of cathode surface; trajectory form 3 was a circle in the central area of cathode surface.

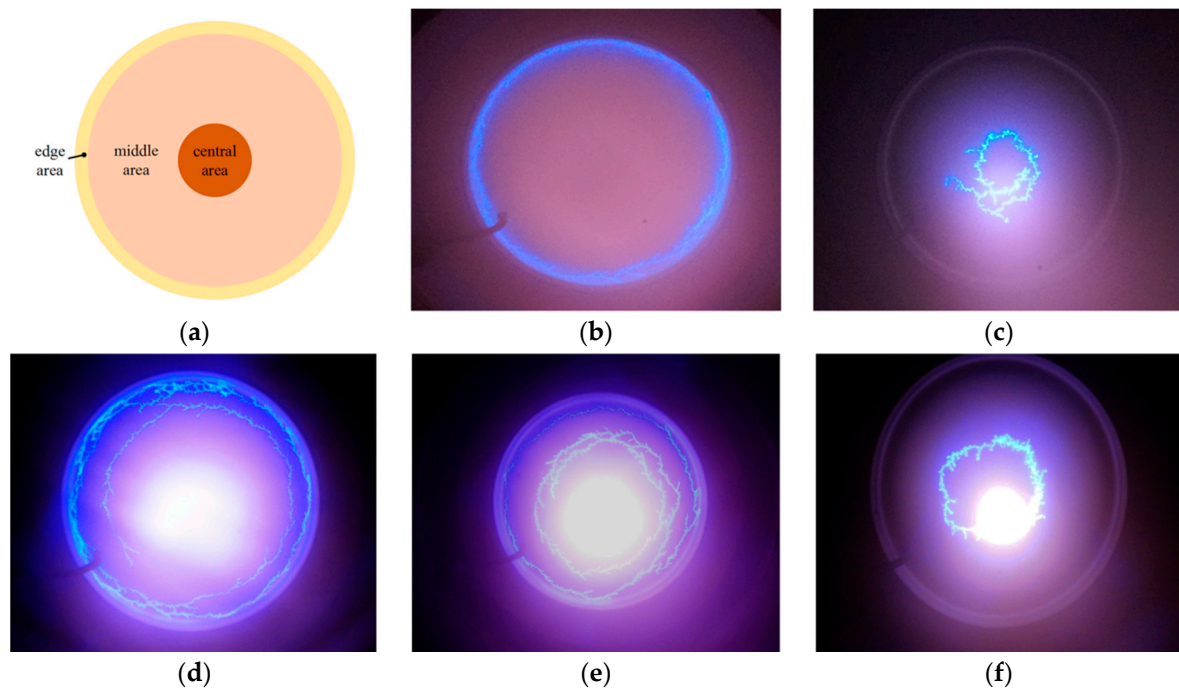


Figure 6. (a) Schematic diagram of cathode spot moving areas with different coil currents; (b) cathode spot trajectory under coil current 0.23 A; (c) cathode spot trajectory under coil current 0.69 A; (d) cathode spot trajectory form 1 with scanning frequency 1 Hz and scanning range 0–0.69 A in stage 1; (e) cathode spot trajectory form 2 with scanning frequency 1 Hz and scanning range 0–0.69 A in stage 2 or 4; (f) cathode spot trajectory form 3 with scanning frequency 1 Hz and scanning range 0–0.69 A in stage 3.

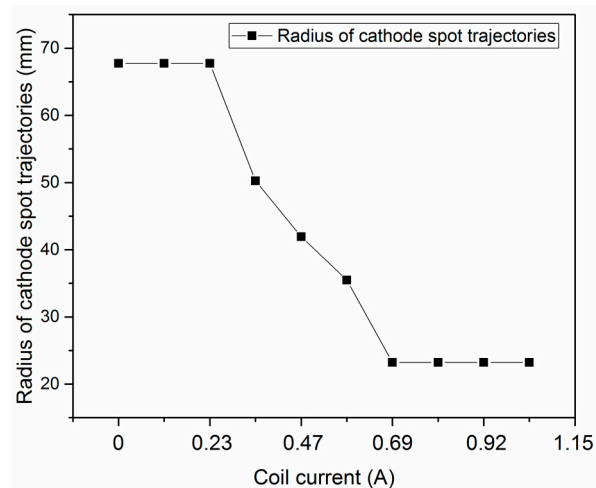


Figure 7. A line chart of radius of trajectory varies with coil current.

Cathode spot velocity was calculated from high-speed camera images. The images were shot continuously with an exposure time of 100 μ s, which allowed imaging distinct spots. Figure 8a–c show three of the sequential images and the time intervals between the images were 100 μ s. It can be seen that the cathode spot moved a tiny distance in these images. So for facilitating analysis, several images were selected from the sequence of images by a fixed and appropriate time interval, which was no more than 1 ms. These images were superimposed to form a composite image. Figure 8d,e show composite images with current of 0.23 A and 0.69 A in the RMF mode. The time interval in Figure 8d,e was 1 ms. Then the angular cathode spot velocity was calculated by counting the number of cathode

spots in one cycle of the composite image. The cathode spot velocity in the RMF was acquired by multiplying the angular velocity by the trajectory radius. Figure 9 presents the variation of cathode spot velocity with different coil currents. It can be found that the velocity first increased then decreased with the coil current and the peak appeared at 0.23 A. In the SRMF mode, an average radial velocity of the cathode spot was used to characterize the radial motion of the cathode spot. Figure 8f presents a composite image during trajectory contraction. The composite image was obtained as the same method introduced above and the time interval was 1 ms. Then, the average values was calculated by s/t . The parameter s represented the radial distance between the edge and the central area, as shown in Figure 8f. The parameter t represented the time of the cathode spot moving during trajectory contraction. This time was calculated by counting the number of cathode spots in the composite image as in Figure 8f. The average radial velocity, during trajectory contraction, varied with the scanning parameters and is plotted in Figure 10. It can be seen from Figure 10 that the contraction velocity of the cathode spot did not significantly vary with the scanning frequency, however it obviously increased with the scanning range.

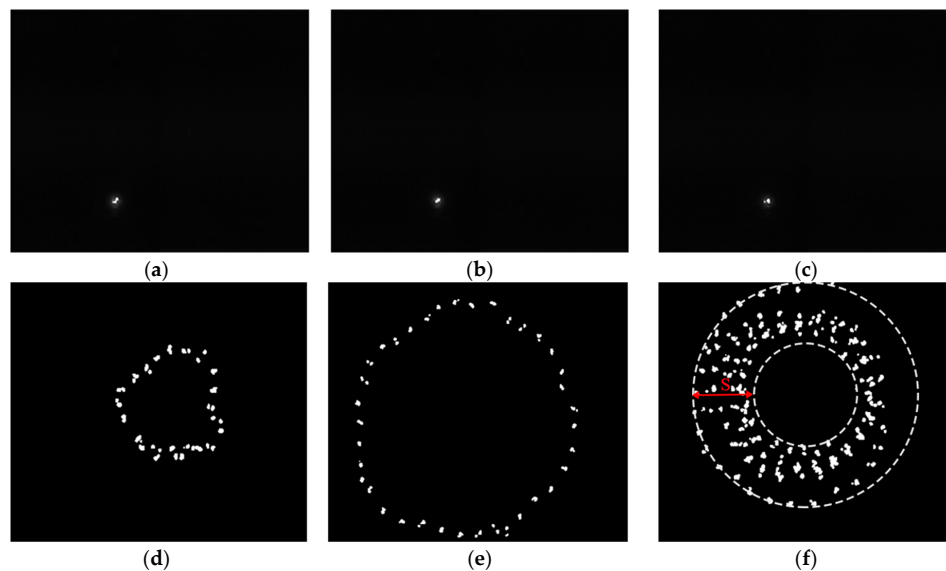


Figure 8. (a) No. 1 of sequential images of cathode spot recorded by a high-speed camera; (b) No. 2 of sequential images of cathode spot recorded by a high-speed camera; (c) No. 3 of sequential images of cathode spot recorded by a high-speed camera; (d) composite image with coil current 0.69 A; (e) composite image with coil current 0.23 A; (f) composite image with scanning frequency 5 Hz, scanning range 0–0.69 A.

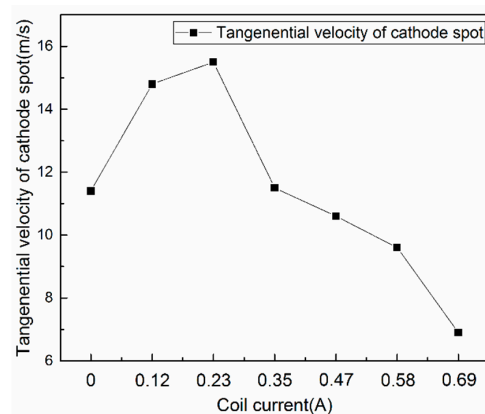


Figure 9. A line chart of the cathode spot tangential velocity varies with coil current.

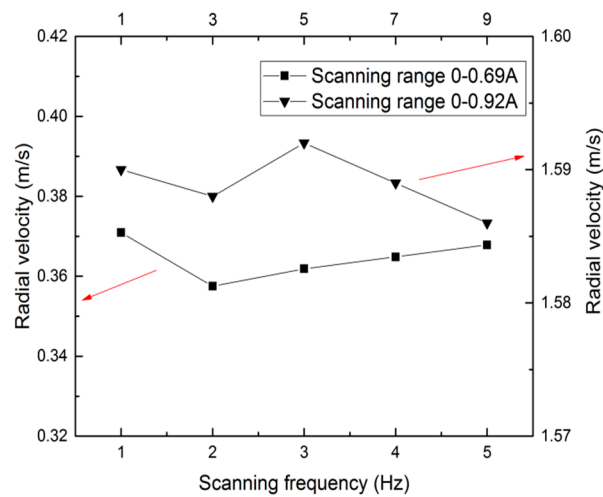


Figure 10. Radial contraction velocity of cathode spot varies with scanning frequency and scanning range.

3.4. Temperature Distribution

Figure 11 presents the cathode surface temperature distribution recorded with a thermal camera. The temperature shown in the images had a deviation from the real temperature of the cathode surface, because of the material emissivity, which depends on the cathode surface condition and is beyond the scope of this paper. In the experiments for the temperature measurement, the deviation kept constant with different magnetic fields. In addition, we mainly focused on the temperature difference. So the real temperature was replaced by the measurement value. The temperature shown in Figure 11a,b was obtained in the RMF mode and Figure 11c,d was in SRMF mode. It can be seen that: (1) the temperature of the cathode spot trajectory with a coil current of 0.23 A was lower than that with 0.69 A; (2) lots of extremely high temperature points gathered in the central area of the cathode surface with coil current 0.69 A; (3) the temperature of the cathode spot trajectory in the SRMF mode was lower than that in the RMF mode; (4) the temperature of the central area with the scanning frequency 1 Hz was higher than that with the scanning frequency 5 Hz, however the temperature of the cathode spot trajectory did not significantly vary with the scanning frequency.

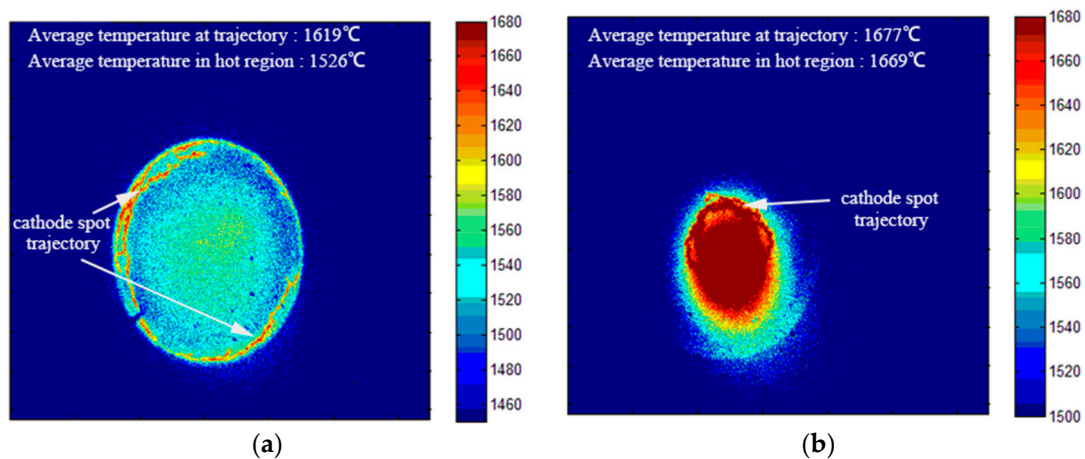


Figure 11. Cont.

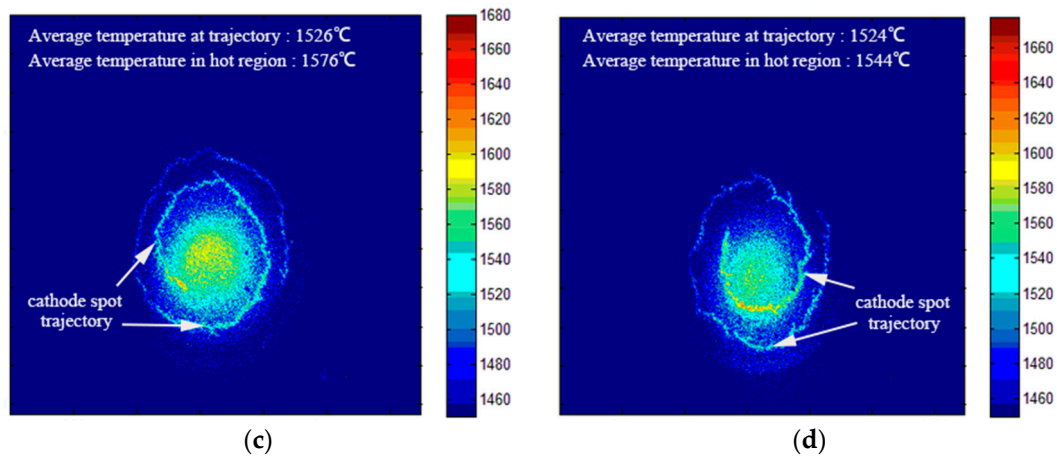


Figure 11. The temperature distribution of cathode surface under different coating parameters: (a) coil current 0.23 A; (b) coil current 0.69 A; (c) scanning frequency 1 Hz, scanning range 0–0.69 A; (d) scanning frequency 5 Hz, scanning range 0–0.69 A.

4. Analysis and Discussion

First, it is important to study the mechanism controlling cathode spot motion in the RMF mode. It is known that the cathode spot will move in retrograde on the cathode surface in a transverse magnetic field [14,16]. Because of the configuration of the RMF, the radial magnetic field B_T was parallel to the cathode surface. So the cathode spot will move in retrograde and perpendicular to the direction of the cathode radius in the RMF and the trajectory will be a circle, as shown in Figure 6b,c. It is known that with the field arched through the cathode surface, the arc moves in the track where the normal field is zero [22]. From Figure 5, it can be seen that the RMF is arched between the center and the edge of the cathode surface and there is usually an annular area with the B_N intensity zero on the cathode surface, when the coil current is between 0.23 and 0.69 A. This “zero area”, or more precisely “zero line”, will contract towards the cathode center, when the coil current increases from 0.23 to 0.69 A. Then the cathode spot trajectory radius will decrease gradually with the coil current. When the coil current is lower than 0.23 A, the cathode spot will be “pushed” towards the edge area, but limited to the cathode surface by the shielding ring shown in Figure 2. At this time, the trajectory is in the cathode surface edge area. When the coil current is higher than 0.69 A, radial field intensity is close to zero at the cathode spot trajectory. Under these conditions, the cathode spot will move randomly in the central area. The variation of the trajectory radius with coil currents matches the experimental results shown in Figure 7. Using the radial magnetic field intensity at the cathode spot position, the variation of cathode spot velocity with the radial magnetic field intensity is shown in Figure 12. It can be seen that the velocity of the cathode spot increased with the radial magnetic field intensity. This agrees with other papers [11,23]. The measured velocity in Ref. [11] was about 15 m/s with the magnetic field intensity 40 Gs and 8 m/s with the magnetic field intensity 17 Gs. In this paper, the measured velocity was 14.8 m/s with the magnetic field intensity 38.3 Gs and 6.9 m/s with the magnetic field intensity 15.8 Gs. So it might be concluded that in the RMF mode, the “zero-line” position of B_N determines the position of the cathode spot trajectory, while the intensity of B_T at the cathode spot determines the cathode spot velocity.

In the SRMF mode, a square scanning waveform was applied to the coil and thus the dynamic behavior of the SRMF can be regarded as a cyclic variation between the low coil (0 A) and high coil (0.69/0.92 A) conditions of the RMF. Then the cathode spot motion in one cycle can be divided into four stages:

- Circular motion in the edge area: when the coil current was in the low condition, the cathode spot moved on the cathode surface edge area, according to the cathode spot motion control mechanism motion in the RMF mode;
- Contraction motion in the middle area: when the coil current changed from the low to the high value, an oblique magnetic field [14,24] appeared at the original position of the cathode spot (at the edge of the cathode surface), as shown in Figure 13a. An acute angle formed between the field vector and cathode surface faced the cathode center. According to the “acute angle rule” [14,22,24], the cathode spot primarily moved in retrograde and secondarily with Robson drift towards cathode center. So the cathode spot moved from the edge to the central area of the cathode surface, at this time;
- Circular motion in the central area: when the coil current was in the high condition, the cathode spot moved on the central cathode area, according to the cathode spot motion control mechanism in the RMF mode;
- Expansion motion in the middle area: when the coil current changed from the high to the low value, an oblique magnetic field appeared at the cathode central area and the acute angle faced the cathode edge, as shown in Figure 13b. At this time, the cathode spot moved from the central to the edge area of the cathode surface.

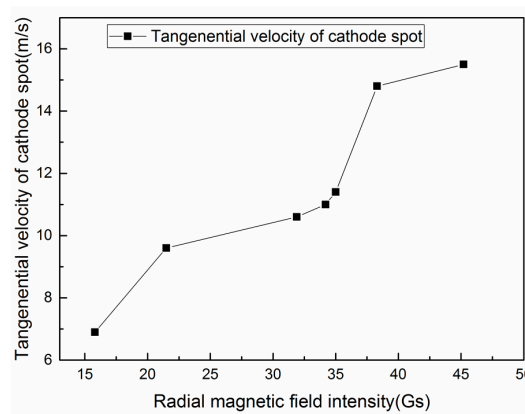


Figure 12. A line chart of varied tangential velocity of cathode spot with radial magnetic field.

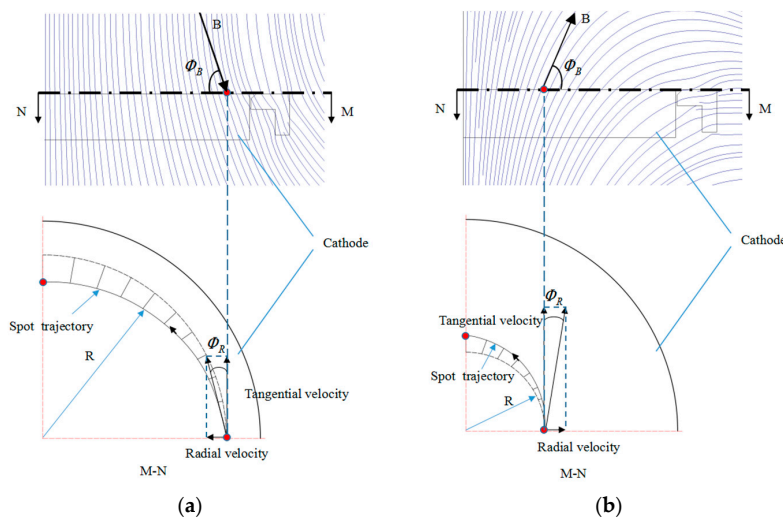


Figure 13. Schematic diagram of the Robson drift on the cathode surface: (a) during trajectory contraction; (b) during trajectory expansion.

So in the SRMF mode, the cathode spot was confined to three different forms. The trajectories of the three forms were shown in Figure 6d–f.

The cathode spot velocity in stage 1 or 3 was the same as that in the RMF mode. The resultant velocity in stage 2 or 4 can be resolved into a tangential velocity v_t and a radial velocity v_r . The tangential velocity v_t increased with the intensity of the radial magnetic field at the cathode spot trajectory according to the control mechanism of cathode spot motion in the RMF mode. It can be seen from Figure 13 that the radial velocity v_r can be expressed by the tangential velocity v_t and the Robson angle \varnothing_R with the formula

$$v_r = v_t \tan \varnothing_R \quad (1)$$

Furthermore, the Robson angle \varnothing_R has a liner relationship with the angle \varnothing_B , which is between the field vector and the cathode surface [25]:

$$\varnothing_R = k\varnothing_B (0.5 \leq k \leq 1) \quad (2)$$

$$\tan \varnothing_B = B_T / B_N \quad (3)$$

According to Equations (1)–(3), the radial velocity is only related to the tangential velocity v_t and the angle \varnothing_B , which are both controlled by the magnetic field intensity. From the above, it can be seen that during trajectory contraction (or expansion), the magnetic field distribution is determined by the immediate value of the coil current. Thus, the scanning frequency does not influence the magnetic field distribution, and the radial velocity will not be affected by the scanning frequency. In this paper, the transition time between the low and high coil condition of the square wave can be neglected. So the contraction (expansion) motion can be regarded as occurring in the high (low) coil current condition of the RMF. If there is a variation of the scanning range, for example, increased from 0–0.69 A to 0–0.92 A, the magnetic field intensity of high coil current condition will be stronger, as shown in Figure 5c. That will cause the tangential and radial velocities of the cathode spot to be larger during trajectory contraction. It might be concluded that the radial velocity of the cathode spot does not significantly vary with the scanning frequency, however it will obviously increase with the scanning range. This is seen in the experiment results shown in Figure 10.

The relationship between the cathode spot motion and the temperature distribution on the cathode surface will now be discussed. Figure 11 shows the distributions of temperature on the cathode surface under different magnetic field parameters. The temperature on the cathode surface will be considered in two regions: at the cathode spot trajectory and inside the cathode spot trajectory. Figure 14a presents the variation of average temperature of the cathode spot trajectory with the cathode spot velocity. It can be seen that the average temperature of the cathode spot trajectory decreased with the cathode spot velocity. This deduction can be explained in two aspects. First, ions gathered near the cathode surface will bombard the cathode surface under the strong electric field, during the arc discharge. This ion bombardment effect will heat the cathode surface. Faster moving velocity of the cathode spot can decrease the ion bombardment time on the spot residence area. Secondly, the cathode spot trajectory is fixed in the RMF mode. So the region of the trajectory is heated by multiple passages of the cathode spot and there will be a large temperature accumulation at the trajectory after a long time arc. Where high cathode spot velocity is experienced, the trajectory radius is larger. That means a larger heated area and a more sufficient cooling effect at the cathode spot trajectory. Then the temperature accumulation will be much smaller. Therefore, the temperature of the cathode spot trajectory decreases with the cathode spot velocity. Furthermore, it can be seen in Figure 11a,b that there is a hot region inside the cathode spot trajectory. Figure 14b shows the variation of average temperature in the hot region with the cathode spot trajectory radius. It can be seen that the average temperature in the hot region decreased with the trajectory radius. Figure 15 shows a schematic diagram of the formation of the hot region inside the cathode spot trajectory. A cathode spot will produce a heat-affected zone (HAZ) on the cathode surface. The HAZ may be regarded as a circular region centered on the cathode spot; its temperature decreases radially. It can be seen in Figure 15 that when the HAZ of

an extinguished cathode spot has not been cooled completely, the newly generated cathode spot brings a new HAZ. Part of these two HAZs overlaps with each other and creates an overlapping HAZ inside the trajectory as shown in Figure 15. The temperature is higher, and the cooling effect is worse in the overlapping region, compared with non-overlapping region. During arcing, heat from the trajectory constantly will diffuse to the overlapping region and raise its temperature. So a hot region will appear inside the cathode spot trajectory after a long time arc. In the RMF mode, the temperature of the cathode spot trajectory is much high, when the radius is small; it diffuses more heat to the hot region. So the temperature of the hot region will become higher with the decrease of the trajectory radius.

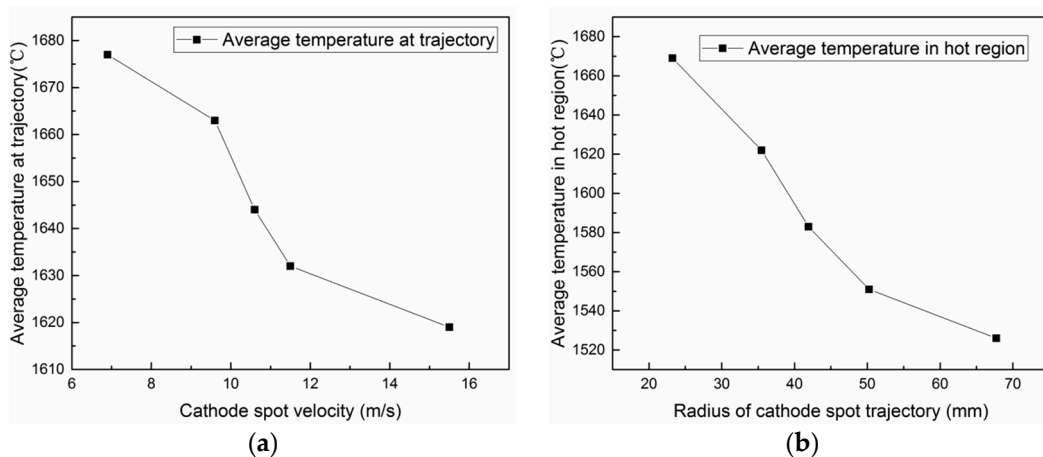


Figure 14. (a) Average temperature of the cathode spot trajectory varies with the cathode spot velocity; (b) average temperature in the hot region varies with cathode spot trajectory radius.

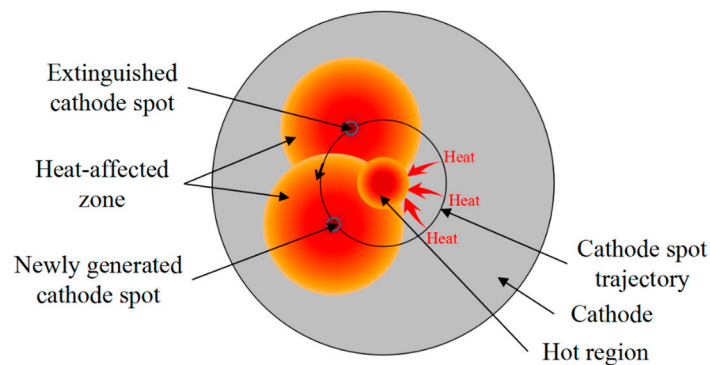


Figure 15. Schematic diagram of the formation of the hot region inside the cathode spot trajectory.

The influence of the temperature on the MP emission is also discussed. It may be conjectured from Figure 4 that the high temperature of the trajectory and in the hot region will increase the emission of MPs. It is said in the literature that the crater formed on the cathode surface coupled with the time-varying plasma pressure produces the MPs [26,27]. A moving cathode spot will produce craters at the cathode trajectory. Higher temperature of the trajectory brings a larger size of the crater. In addition, a larger size crater may increase the MP emission. The hot region near the cathode spot may increase thermionic and vaporized electrode material emission and consequently the density of metal ions near the cathode surface [19,27]. The higher the temperature in the hot region is, the stronger the plasma pressure will be. So it will bring not only large amount but also big diameter of MPs, combined with a large size of the crater. The schematic diagram of the generation process of the MPs is shown in Figure 16.

The influence of the SRMF on the MP reduction can be explained by the influence of the cathode spot motion on the temperature distribution of the cathode surface. Using SRMF, the cathode spot moves over a larger area, which avoids the cathode surface being heated by multiple passages of the cathode spot in comparison with the RMF. In the SRMF mode, the temperature of the cathode spot trajectory with scanning frequency 1 Hz is not too different from that with scanning frequency 5 Hz. However, the temperature of the hot region with scanning frequency 1 Hz is higher than that with scanning frequency 5 Hz shown in Figure 11c,d. This is because the whole residence time of the cathode spot in stage 3 during deposition decreases with the scanning frequency. So the overall quantity and average diameter of MPs decreased with the scanning frequency, when the scanning range was fixed. When the scanning range changes to 0–0.92 A, the cathode spot moves faster; it will further decrease the temperature on the cathode surface and reduce the MP emission.

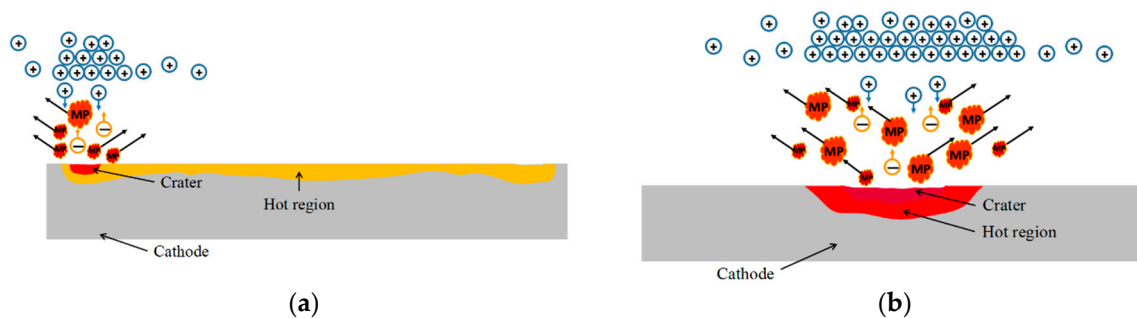


Figure 16. Schematic diagram of the generation process of the MPs with different coil currents: (a) 0.23 A; (b) 0.69 A.

5. Conclusions

The SRMF was proposed to control cathode spot motion and reduce the emission of the MPs. The mechanism of the SRMF on reduced MP emission was explained by establishing a correlation between the SRMF cathode spot motion and the MP emission affected by the temperature distribution on the cathode surface.

In the SRMF mode, the cathode spot motion can be divided into four stages: circular motion in the edge area of the cathode surface, contraction motion in the middle area of the cathode surface, circular motion in the central area of the cathode surface and expansion motion in the middle area of the cathode surface. The radial velocity of the cathode spot, during trajectory contraction (or expansion) was determined by the magnetic field distribution on the cathode surface. It did not significantly vary with the scanning frequency, however it will obviously increase with the scanning range.

The temperature of the cathode spot trajectory decreased with the cathode spot velocity and the temperature of the hot region became higher with the decrease of the trajectory radius. The SRMF mode produced a lower temperature of the trajectory and in the hot region of the cathode surface.

By using SRMF, the quantity and size of the MPs was decreased in comparison with using RMF. The improvement was greater with increased scanning range and frequency.

Acknowledgments: This work was supported by National Natural Science Foundation of China (51775096), Fundamental Research Funds for the Central Universities, China (N141008001/2), and the grants (Y17-0-003 and F16-080-8-00) from Shenyang city.

Author Contributions: Shuhao Wang, Dechun Ba and Zeng Lin conceived and designed the experiments; Dechun Ba designed and developed the equipment; Hong Qiao performed the experiments; Shuhao Wang, Hong Qiao and Lida Zhu analyzed the data; Shuhao Wang and Zeng Lin wrote the paper.

Conflicts of Interest: The authors declare no conflict of interest.

References

1. Brown, I.G. Cathodic arc deposition of films. *Annu. Rev. Mater. Res.* **1998**, *28*, 243–269. [[CrossRef](#)]
2. Vetter, J. Vacuum arc coatings for tools: Potential and application. *Surf. Coat. Technol.* **1995**, *76*, 719–724. [[CrossRef](#)]
3. Knotek, O.; Bohmer, M.; Leyendecker, T. On structure and properties of sputtered Ti and Al-based hard compound films. *J. Vac. Sci. Technol. A Vac. Surf. Films* **1986**, *4*, 2695–2700. [[CrossRef](#)]
4. Heidsieck, H. Status of vacuum and plasma technology. *Surf. Coat. Technol.* **1999**, *112*, 324–338. [[CrossRef](#)]
5. Ramalingam, S. Emerging applications and new opportunities with PVD Arc sources. In *Handbook of Vacuum Arc Science and Technology*; Boxman, R.L., Sanders, D.M., Martin, P.J., Eds.; William Andrew Publishing: Norwich, NY, USA, 1996; pp. 519–551.
6. Li, L.; Zhu, Y.; He, F.; Dun, D.; Li, F.; Chu, P.K. Control of cathodic arc spot motion under external magnetic field. *Vacuum* **2013**, *91*, 20–23. [[CrossRef](#)]
7. Aksenov, I.I.; Belokhvostikov, A.N.; Padalka, V.G.; Repalov, N.S.; Khoroshikh, V.M. Plasma flux motion in a toroidal plasma guide. *Plasma Phys. Control. Fusion* **1986**, *28*, 761–770. [[CrossRef](#)]
8. Aksenov, I.I.; Strel'nitskij, V.E.; Vasilyev, V.V.; Zaleskij, D.Y. Efficiency of magnetic plasma filters. *Surf. Coat. Technol.* **2003**, *163*, 118–127. [[CrossRef](#)]
9. Zhang, T.; Kwok, D.T.K.; Chu, P.K.; Brown, I.G. Guiding effects of electric and magnetic fields on the plasma output of a cathodic arc magnetic filter. *J. Appl. Phys.* **2001**, *89*, 672–675. [[CrossRef](#)]
10. Bizyukov, A.A.; Chibisov, D.V.; Chibisov, A.D.; Romashchenko, E.V.; Kovalenko, V.V. Dynamics of macroparticles in a magnetic filter for a vacuum arc plasma sources. *Probl. At. Sci. Technol.* **2015**, *4*, 298–301.
11. Swift, P.D.; Mckenzie, D.R.; Falconer, I.S.; Martin, P.J. Cathode spot phenomena in titanium vacuum arcs. *J. Appl. Phys.* **1989**, *66*, 505–512. [[CrossRef](#)]
12. Swift, P.D. Macroparticles in films deposited by steered cathodic arc. *J. Phys. D Appl. Phys.* **1996**, *29*, 2025–2031. [[CrossRef](#)]
13. Lang, W.C. Design of a dynamic magnetic field steered cathodic arc source in arc ion plating. *Adv. Mater. Res.* **2012**, *340*, 167–172. [[CrossRef](#)]
14. Lang, W.C.; Cao, Y.; Du, H.; Wang, X.H. Effect of multi-mode dynamic coupling magnetic field on arc spots movement in arc ion plating. *Metall. Min. Ind.* **2015**, *35*, 662–670.
15. Boxman, R.L.; Gerby, E.; Goldsmith, S. Behavior of a high current vacuum arc between hollow cylindrical electrodes in a radial magnetic field. *IEEE Trans. Plasma Sci.* **1980**, *8*, 308–313. [[CrossRef](#)]
16. Ramalingam, S.; Qi, C.B.; Kim, K. Controlled vacuum arc material deposition, method and apparatus. U.S. Patent 4673477 A, 16 June 1987.
17. Zhirkov, I.; Petruhins, A.; Rosen, J. Effect of cathode composition and nitrogen pressure on macroparticle generation and type of arc discharge in a DC arc source with Ti-Al compound cathodes. *Surf. Coat. Technol.* **2015**, *281*, 20–26. [[CrossRef](#)]
18. Jüttner, B. On the variety of cathode craters of vacuum arcs, and the influence of the cathode temperature. *Physica B+C* **1982**, *114*, 255–261. [[CrossRef](#)]
19. Anders, A. *Cathodic Arcs*; Springer: New York, NY, USA, 2008.
20. Utsumi, T.; English, J.H. Study of electrode products emitted by vacuum arcs in form of molten metal particles. *J. Appl. Phys.* **1975**, *46*, 126–131. [[CrossRef](#)]
21. Gellert, B.; Schade, E. Optical investigation of droplet emission in vacuum interrupters to improve contact materials. In Proceedings of the 14th International Symposium on Discharges and Electrical Insulation in Vacuum, Santa Fe, NM, USA, 16–20 September 1990; pp. 450–454.
22. Boxman, R.L.; Beilis, I.I.; Gidalevich, E.; Zhitomirsky, V.N. Magnetic control in vacuum arc deposition: A review. *IEEE Trans. Plasma Sci.* **2005**, *33*, 1618–1625. [[CrossRef](#)]
23. Boxman, R.L.; Goldsmith, S.; Greenwood, A. Twenty-five years of progress in vacuum arc research and utilization. *IEEE Trans. Plasma Sci.* **2002**, *25*, 1174–1186. [[CrossRef](#)]
24. Lang, W.C.; Xiao, J.Q.; Gong, J.; Sun, C.; Huang, R.F.; Wen, L.S. Study on cathode spot motion and macroparticles reduction in axisymmetric magnetic field-enhanced vacuum arc deposition. *Vacuum* **2010**, *84*, 1111–1117. [[CrossRef](#)]
25. Boxman, R.L. Handbook of vacuum arc science and technology. *Geochim. Cosmochim. Acta* **1996**, *46*, 2039–2047.

26. Kuznetsov, V.G.; Babushkina, E.S. Mathematical modeling of the temperature distribution under the cathode spot of the vacuum arc. *J. Phys. Conf. Ser.* **2016**, *729*, 012003. [[CrossRef](#)]
27. McClure, G.W. Plasma expansion as a cause of metal displacement in vacuum-arc cathode spots. *J. Appl. Phys.* **1974**, *45*, 2078–2084. [[CrossRef](#)]



© 2018 by the authors. Licensee MDPI, Basel, Switzerland. This article is an open access article distributed under the terms and conditions of the Creative Commons Attribution (CC BY) license (<http://creativecommons.org/licenses/by/4.0/>).